

Domain Alignment and Temporal Aggregation for Unsupervised Video Object Segmentation

Suhwan Cho^{1,*} Minhyeok Lee^{1,*} Seunghoon Lee¹ Sangyoun Lee^{1,2}

¹ Yonsei University

² Korea Institute of Science and Technology (KIST)

Abstract

Unsupervised video object segmentation aims at detecting and segmenting the most salient object in videos. In recent times, two-stream approaches that collaboratively leverage appearance cues and motion cues have attracted extensive attention thanks to their powerful performance. However, there are two limitations faced by those methods: 1) the domain gap between appearance and motion information is not well considered; and 2) long-term temporal coherence within a video sequence is not exploited. To overcome these limitations, we propose a domain alignment module (DAM) and a temporal aggregation module (TAM). DAM resolves the domain gap between two modalities by forcing the values to be in the same range using a cross-correlation mechanism. TAM captures long-term coherence by extracting and leveraging global cues of a video. On public benchmark datasets, our proposed approach demonstrates its effectiveness, outperforming all existing methods by a substantial margin. Code and models are available at <https://github.com/Hydragon516/DATA>.

1. Introduction

Video object segmentation (VOS) is a fundamental task in computer vision. Given a video sequence as input, the objective is to segment objects for entire frames. It can be divided into several categories depending on how the objects to be detected are defined. If they are defined by the initial frame segmentation mask, the task is called semi-supervised VOS. If human interaction is used for object guidance, it is called interactive VOS, whereas if there is no guidance, it is called unsupervised VOS. In this study, we deal with the unsupervised setting, i.e., detecting and segmenting the most salient object in a video sequence without any external guidance.

In unsupervised VOS, two-stream approaches, such as

*These authors contribute equally to this work.

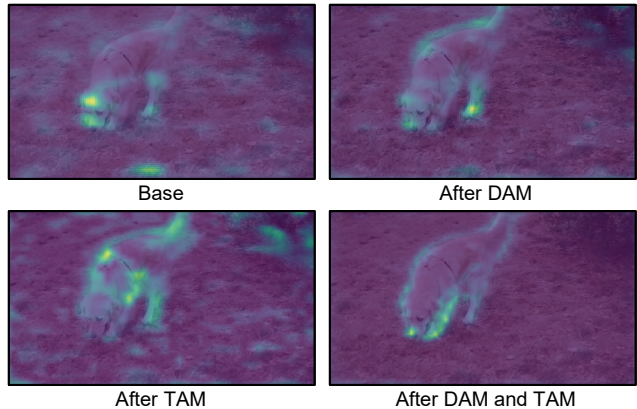


Figure 1. Visualized feature maps of various embedding stages.

MATNet [33], FSNet [4], and HFAN [14], have been recently attracting extensive attention thanks to their effectiveness at capturing distinctive objects in videos. For each video frame, an RGB image and an optical flow map generated by pre-trained optical flow estimation models are used as input to provide appearance and motion information simultaneously. To effectively fuse the multi-modal cues, existing methods mainly focus on designing a mutual reciprocity method that directly blends the embedded features obtained from each modality. Although multi-modal cues can be leveraged to a certain extent, two concerns remain. First, the domain gap between appearance cues and motion cues is not considered. Appearance and motion cues are directly fused using naive feature summation or concatenation, which causes noisy and incorrect prediction. Second, long-term coherence of videos cannot be considered. As only a single-frame RGB image and an optical flow map are used as input, only short-term information can be exploited, which makes the system susceptible to object occlusions. In this study, we introduce two novel modules to overcome such limitations of existing two-stream approaches.

As described, a direct fusion between appearance and motion cues is not effective enough as their domains

have different properties. In order to appropriately fuse multi-modal cues, we propose a domain alignment module (DAM) that aligns and then blends the appearance and motion cues. Instead of applying a naive summation or concatenation to multi-modal features, we first construct prototype features from each modality similar to OCR [29]. Then, self-correlation maps are generated by comparing the generated prototype features and input features for each separate modality. Finally, the self-correlation maps, which have the same value range, provide mutual guidance to each other using a conventional attention mechanism. Based on the similarity between key features, value features are propagated to different modalities. Through this process, salient regions showing high confidence in both modalities can be highlighted. The propagated features are fused with the input features, and refined features can be obtained.

As salient objects usually show distinctive movements over the background, jointly using appearance and motion cues is an effective strategy for unsupervised VOS. However, for challenging scenarios where salient objects are partially occluded, the single-frame approach is not effective. To deal with such cases, we propose a temporal aggregation module (TAM) that leverages the global context of a video sequence for prediction of each single frame. To this end, we first construct an external memory pool that stores key and value features of the sampled frames from the entire sequence. When predicting a query frame, memory value features are transferred to the query frame based on the correlation between memory key features and query key features. Even if the target object is partially occluded, reliable features extracted from a holistic view can be allocated to it by an attention mechanism.

We evaluate our proposed approach on three popular benchmark datasets for unsupervised VOS, DAVIS 2016 [15] validation set, FBMS [13] test set, and YouTube-Objects [16] dataset. On all of them, our method surpasses all existing methods by a substantial margin. Extensive experiments are also conducted to demonstrate the effectiveness of the proposed components.

Our main contributions can be summarized as follows:

- We propose a DAM to reduce the domain gap between appearance cues and motion cues. The features from each domain are first aligned and then fused with each other.
- We propose a TAM to fully exploit the temporal property of a video. The global context for a video sequence is propagated to each separate frame and used for prediction.
- On all public benchmark datasets, our approach sets a new state-of-the-art performance, while not avoiding high computational complexity.

2. Related Work

Two-stream architecture. In unsupervised VOS, two-stream architectures that jointly leverage appearance cues and motion cues have been attracting extensive attention. MATNet [33] designs a two-stream encoder that utilizes an RGB image and an optical flow map to enhance spatio-temporal object representation. RTNet [17] proposes a reciprocal transformation network to identify and segment primary objects in videos. FSNet [4] proposes a full-duplex strategy to effectively fuse RGB images and optical flow maps; specifically, a bidirectional interaction module is used to ensure the mutual restraint between appearance and motion cues. AMC-Net [27] proposes a co-attention gate that modulates the impacts of appearance and motion cues. Based on the learned weights, appearance and motion information can be leveraged adaptively. TransportNet [30] establishes the correspondence between appearance and motion cues while suppressing the distractions via optimal structural matching. HFAN [14] proposes a hierarchical feature alignment network that aligns the object positions using the appearance and motion features. The cross-modal mismatch can be mitigated by adapting the aligned features. PMN [7] stores prototype features of appearance cues as well as and motion cues to fully leverage multiple modalities. TMO [3] optionally employs a motion stream on top of an appearance stream to adaptively leverage motion information. Although these two-stream methods are effective at capturing primary objects showing distinctive movements, the performance can be further improved by relieving two factors: 1) the domain gap between appearance features and motion features; 2) overlooking of the temporal coherence within a video. By adopting our proposed DAM, these concerns can be effectively addressed.

Temporal coherence. There are also studies that solve the unsupervised VOS problem without employing motion cues from optical flow estimation. Unlike existing two-stream methods, they mainly focus on fully exploiting the temporal coherence of a video. COSNet [11] employs the co-attention layers to capture global correlations and scene context by propagating semantic information in the reference frames to the query frame. AGNN [24] builds fully connected graphs to represent frames as nodes and relations between those frames as edges. Rich relations between arbitrary frames can be obtained through parametric message passing. AD-Net [28] and F2Net [9] regards the initial frame of a video as a reference frame, and leverages the reference frame information for query frame prediction. IMP [8] iteratively propagates the segmentation mask of an easy reference frame to other frames by using a pre-trained semi-supervised VOS algorithm. These methods can capture temporal coherence in a video, but still suffer from certain problems such as the global context of a video not

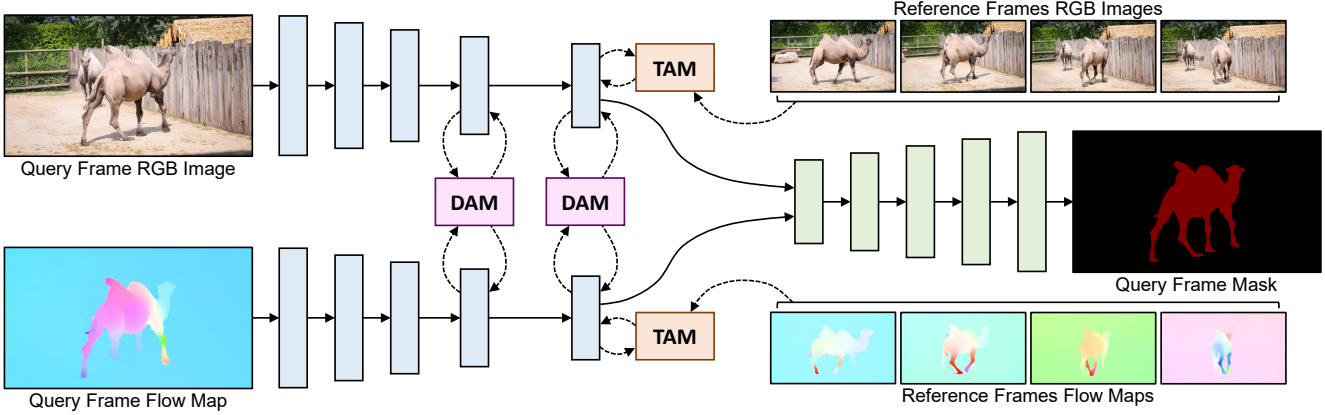


Figure 2. Architecture of our proposed network. Based on a two-stream encoder–decoder architecture that simultaneously leverages RGB image and optical flow map, domain alignment and temporal aggregation modules are adopted. For simplicity, skip connections between encoding blocks and decoding blocks are omitted in the illustration.

being completely leveraged and requiring heavy computational complexity owing to the iterative inferring process. By contrast, our proposed TAM can leverage the temporal coherence of a video while not suffering such issues.

3. Approach

3.1. Problem Formulation

The goal of an unsupervised VOS algorithm is to identify the most salient object for all frames of a video. Following common protocol in the VOS community, we collaboratively use RGB images and optical flow maps as the input of our network. The network output is binary segmentation masks that have the same resolution as the input information. RGB images, optical flow maps, and output segmentation masks are denoted as $I := \{I^0, I^1, \dots, I^{L-1}\}$, $F := \{F^0, F^1, \dots, F^{L-1}\}$, and $O := \{O^0, O^1, \dots, O^{L-1}\}$, respectively, where L is the number of total frames.

3.2. Network Architecture

Like existing two-stream approaches for unsupervised VOS, such as MATNet [33], FSNet [4], HFAN [14], PMN [7], and TMO [3], our network is based on a simple encoder–decoder architecture that both RGB image and optical flow map as inputs and outputs a binary segmentation mask. In the middle of the encoding and decoding process, the proposed DAM and TAM are adopted for domain alignment and temporal cue aggregation. The visualized pipeline of our network can be found at Figure 2.

3.3. Domain Alignment Module

Existing two-stream approaches, including the aforementioned methods, focus on effectively fusing the multi-modal cues. However, they simply sum or concatenate the multi-modal features lying in different feature domains,

which limits the effectiveness of the joint use of multiple modalities. To maximize the efficacy of multi-modal fusion in unsupervised VOS, we propose a DAM for better fusing and exploiting multi-modal features. The proposed DAM consists of three parts: prototype generation, self-correlation calculation, and mutual feature refinement. In Figure 3, we visualize the architecture of DAM.

Prototype generation. Inspired by OCR [29], we first generate prototype features based on learnable object regions. For each input feature map $X \in \mathbb{R}^{C \times HW}$, soft object region $S \in [0, 1]^{C \times HW}$ is calculated by applying a simple channel-wise softmax operation as

$$S = \text{Softmax}(X). \quad (1)$$

Considering the encoder is learned with large-scale ImageNet [6], each channel in S already contains the clustering ability that helps separate the input feature map into semantic parts spatially. Then, using X and S , prototype features $P \in \mathbb{R}^{C \times C'}$ are obtained as

$$P = X \otimes S^{-1}, \quad (2)$$

where \otimes indicates matrix multiplication. In P , C' prototypes with a channel size of C are contained. Note that C' is equal to C , but is adopted for better clarification.

Self-correlation calculation. In order to effectively fuse appearance information and motion information, we need to locate them in the same feature domain and then exchange the respective cues. To this end, instead of directly blending their features, we first calculate self-correlation map $\Psi 1 \in [-1, 1]^{C' \times HW}$ for each of them as

$$\Psi 1 = \mathcal{N}(P)^{-1} \otimes \mathcal{N}(X), \quad (3)$$

where \mathcal{N} indicates channel L2 normalization. The generated $\Psi 1$ represents the cosine similarities between each prototype feature and each input feature. As the value range

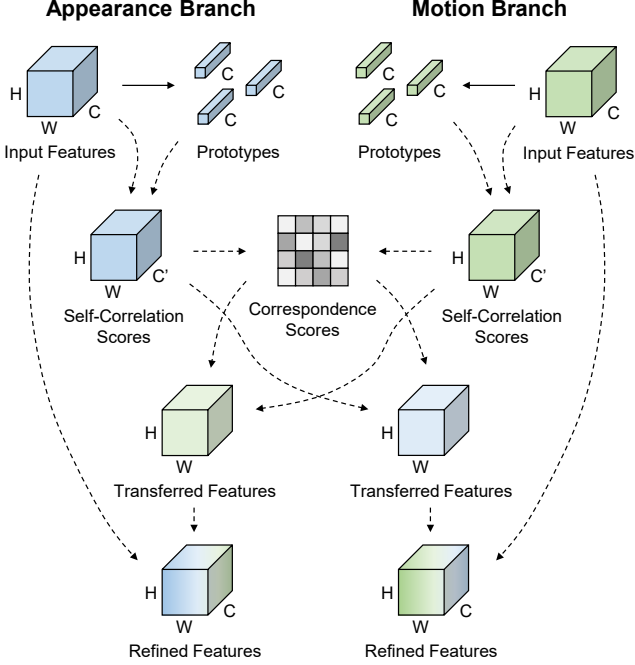


Figure 3. Visualized pipeline of domain alignment module.

of Ψ_1 is identical for the appearance stream as well as the motion stream, it can be said that the self-correlation maps of the appearance stream and motion stream share the same feature space. The appearance–motion fusion in this “aligned” domain is much more effective and reliable than the fusion in “unique” domains as it does not suffer from a domain gap that may cause certain biases.

Mutual feature refinement. After calculating the correlation scores and generating the self-correlation maps for each modality, the information of each modality can now be effectively transferred to each other in the “aligned” domain using an attention mechanism. From Ψ_1 , the key features $K \in \mathbb{R}^{C' \times N}$ and value features $V \in \mathbb{R}^{C' \times M}$ are first calculated as

$$\begin{aligned} K &= \sigma_K(\Psi_1) \\ V &= \sigma_V(\Psi_1), \end{aligned} \quad (4)$$

where σ indicates a channel-wise (C' -wise) fully-connected layer. Next, the correspondence map $\Phi_1 \in \mathbb{R}^{C' \times C'}$ of the key features of each modality, i.e., $K_A \in \mathbb{R}^{C' \times N}$ and $K_M \in \mathbb{R}^{C' \times N}$, are computed as

$$\Phi_1 = K_A \otimes K_M^{-1}. \quad (5)$$

Based on Φ , V from one modality are propagated to the other modality as

$$\begin{aligned} T_A &= \text{Softmax}(\Phi_1) \otimes V_M \\ T_M &= \text{Softmax}(\Phi_1^{-1}) \otimes V_A, \end{aligned} \quad (6)$$

where T indicates the transferred features. Finally, the input features are concatenated with the transferred features, and the refined features $X' \in \mathbb{R}^{C \times HW}$ are obtained as

$$\begin{aligned} X'_A &= \text{Conv}(X_A \oplus T_A) \\ X'_M &= \text{Conv}(X_M \oplus T_M), \end{aligned} \quad (7)$$

where \oplus indicates channel concatenation. Conv is a convolutional layer for feature refinement. Through this mutual refinement process, each modality can appropriately reflect semantic information from another modality, while preventing the inevitable occurrence of a domain gap problem.

3.4. Temporal Aggregation Module

As much as aligning the feature domains of multiple modalities is important, exploiting temporal coherence of a video is also an effective strategy for unsupervised VOS. Existing approaches, such as COSNet [11], AD-Net [28], F2Net [9], and IMP [8], design their network architectures to utilize this temporal coherence. However, they are either time-consuming owing to their iterative workflows or not fully leveraging the global context of a video. To overcome these limitations, we propose a TAM to efficiently leverage the temporal coherence of a video. The proposed TAM consists of three parts: reference frame sampling, prototype generation, and temporal propagation. In Figure 4, we visualize the architecture of TAM.

Reference frame sampling. The objective of TAM is to collect and store the global context of a video and propagate it to each query frame. To efficiently obtain the global context, we sample the frames in a video and selectively store the sampled frames rather than storing all frames. As the sampling method, we adopt the uniform sampling strategy, i.e., the frames are sampled while keeping the intervals identical. For example, if we want to sample N frames from the L -length video, the sampled frames are defined as $\{I^k\}_{i=0}^{N-1}$ where

$$k = \lfloor \frac{i * (L - 1)}{N - 1} \rfloor. \quad (8)$$

Temporal context propagation. After selecting representative frames from a video, we transfer the semantic context obtained from the reference frames to each query frame. Given that input features of TAM are denoted as $Y \in \mathbb{R}^{D \times HW}$, query features are embedded from Y of the query frame, while key and value features are embedded from Y of the reference frames. Similar to *prototype generation* at Section 3.3, query prototype features $P^Q \in \mathbb{R}^{D \times D'}$, key prototype features $P^K \in \mathbb{R}^{D \times ND'}$, and value prototype features $P^V \in \mathbb{R}^{D \times ND'}$ are embedded from key features, query features, and value features, respectively. Then, the correspondence map $\Phi_2 \in \mathbb{R}^{D' \times ND'}$ is generated as

$$\Phi_2 = P^{Q^{-1}} \otimes P^K. \quad (9)$$

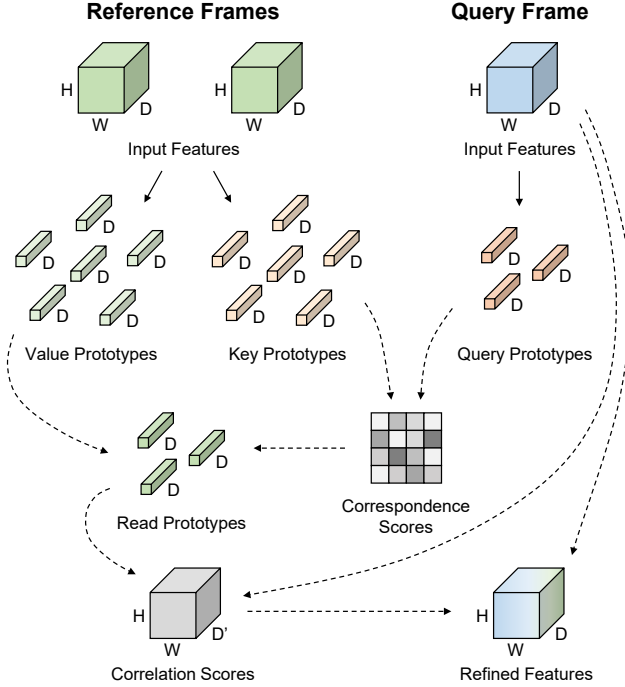


Figure 4. Visualized pipeline of temporal aggregation module.

Based on $\Phi 2$, the context of the reference frames are adaptively read and stored in read prototype features $R \in \mathbb{R}^{D \times D'}$ as

$$R = (\text{Softmax}(\Phi 2) \otimes P^{V^{-1}})^{-1}. \quad (10)$$

The generated R can be interpreted as having D' prototypes with feature size of D . As it does not have spatial information, it cannot be directly leveraged for the feature fusion process. Therefore, we calculate the correlation scores $\Psi 2 \in [-1, 1]^{D' \times HW}$ between Y and R to force the temporally transferred information to have the same spatial size as the input features, as follows:

$$\Psi 2 = \mathcal{N}(R)^{-1} \otimes \mathcal{N}(Y). \quad (11)$$

As Y and R have the same spatial size, feature fusion between them can now be easily achieved. The refined features $Y' \in \mathbb{R}^{D \times HW}$ is defined as

$$Y' = \text{Conv}(Y \oplus \Psi 2). \quad (12)$$

By employing the proposed DAM, the semantic context of the reference frames is propagated to the query frame for reliable cue generation. In particular, when reliable information cannot be obtained from a single frame owing to occlusions, cues obtained from temporally global observation can be leveraged, which leads to stable functioning of a system.

3.5. Implementation Details

Optical flow map. Following a common protocol for two-stream approaches in unsupervised VOS, we generate optical flow maps from a pre-trained optical flow estimation model. The generated two-channel motion flow maps are converted to three-channel RGB flow maps and then saved in advance. As an optical flow estimation model, we adopt RAFT [22] pre-trained on the Sintel [1] dataset.

Network design. We adopt VGG-16 [20] as our backbone encoder for the appearance branch and motion branch. The encoded features are refined using DAM and TAM, where DAM is adopted for the fourth and fifth encoding blocks and TAM is adopted at the fifth encoding block. Note that DAM and TAM are separately adopted in the fifth encoding block, that is, they are employed in a parallel manner and then fused later. After refining the encoded features using DAM and TAM, an ASPP module [2] is applied to obtain stronger feature representations. The decoder takes the features from the ASPP module as its input, and gradually refines those features using lower-level features from the encoder.

Two-stage network training. Following previous methods, such as F2Net [9], RTNet [17], FSNet [4], and PMN [7], we train our network using multiple steps. As the first step, a salient object detection dataset DUTS [23] is adopted to pre-train the model on large-scale data. Both DUTS training set and test set are used as our training dataset. As it is an image-level dataset, only RGB images are available. Therefore, we only train the appearance branch and copy the learned parameters to the motion branch after the pre-training is done. Then, the entire model is trained on the DAVIS 2016 [15] training set and YouTube-VOS 2018 [26] training set with appearance as well as motion branches turned on. If a video sequence contains multiple objects, we regard them as a single object to obtain binary ground truth masks. Training snippets are randomly sampled from the DAVIS 2016 training set and YouTube-VOS 2018 training set with the same probabilities.

Training details. For network optimization, we use cross-entropy loss and the Adam optimizer [5]. The learning rate is decayed from $1e-4$ to $1e-5$ using the cosine annealing scheduler [10], and the batch size is set to 16. For network training, two GeForce RTX 3090 GPUs are used.

4. Experiments

In this section, the datasets used in this study are first introduced in Section 4.1. Quantitative and qualitative comparison with other methods can be found at Section 4.3 and Section 4.4, respectively. Finally, each proposed component is analyzed in Section 4.5. Note that our method is abbreviated as DATA.

Table 1. Quantitative evaluation on the DAVIS 2016 validation set and FBMS test set. OF and PP indicate the use of optical flow estimation models and post-processing techniques, respectively.

Method	Publication	Resolution	OF	PP	fps	DAVIS 2016			FBMS
						\mathcal{G}_M	\mathcal{J}_M	\mathcal{F}_M	\mathcal{J}_M
PDB [21]	ECCV'18	473×473		✓	20.0	75.9	77.2	74.5	74.0
MOTAdapt [19]	ICRA'19	-		✓	-	77.3	77.2	77.4	-
AGS [25]	CVPR'19	473×473		✓	10.0	78.6	79.7	77.4	-
COSNet [11]	CVPR'19	473×473		✓	-	80.0	80.5	79.4	75.6
AD-Net [28]	ICCV'19	480×854		✓	4.00	81.1	81.7	80.5	-
AGNN [24]	ICCV'19	473×473		✓	3.57	79.9	80.7	79.1	-
MATNet [33]	AAAI'20	473×473	✓	✓	20.0	81.6	72.4	80.7	76.1
WCS-Net [31]	ECCV'20	320×320			<u>33.3</u>	81.5	82.2	80.7	-
DFNet [32]	ECCV'20	-		✓	3.57	82.6	83.4	81.8	-
3DC-Seg [12]	BMVC'20	480×854		✓	4.55	84.5	84.3	84.7	-
F2Net [9]	AAAI'21	473×473			10.0	83.7	83.1	84.4	77.5
RTNet [17]	CVPR'21	384×672	✓	✓	-	85.2	85.6	84.7	-
FSNet [4]	ICCV'21	352×352	✓	✓	12.5	83.3	83.4	83.1	-
TransportNet [30]	ICCV'21	512×512	✓		12.5	84.8	84.5	85.0	78.7
AMC-Net [27]	ICCV'21	384×384	✓	✓	17.5	84.6	84.5	84.6	76.5
D ² Conv3D [18]	WACV'22	480×854			-	86.0	85.5	86.5	-
IMP [8]	AAAI'22	-			1.79	85.6	84.5	86.7	77.5
HFAN [14]	ECCV'22	512×512	✓		12.4	<u>87.0</u>	<u>86.6</u>	87.3	-
PMN [7]	WACV'23	352×352	✓		-	85.9	85.4	86.4	77.7
TMO [3]	WACV'23	384×384	✓		43.2	86.1	85.6	86.6	<u>79.9</u>
DATA		352×352	✓		25.4	86.9	86.3	<u>87.4</u>	78.9
DATA		512×512	✓		20.2	87.6	87.1	88.2	81.0

Table 2. Quantitative evaluation on the YouTube-Objects dataset. Performance is reported using the \mathcal{J} mean.

Method	Aeroplane	Bird	Boat	Car	Cat	Cow	Dog	Horse	Motorbike	Train
PDB [21]	78.0	80.0	58.9	76.5	63.0	64.1	70.1	67.6	58.4	35.3
AGS [25]	87.7	76.7	72.2	78.6	69.2	64.6	73.3	64.4	62.1	48.2
COSNet [11]	81.1	75.7	71.3	77.6	66.5	69.8	76.8	67.4	67.7	46.8
AGNN [24]	71.1	75.9	70.7	78.1	67.9	69.7	<u>77.4</u>	67.3	<u>68.3</u>	47.8
MATNet [33]	72.9	77.5	66.9	79.0	73.7	67.4	75.9	63.2	62.6	51.0
WCS-Net [31]	81.8	<u>81.1</u>	67.7	79.2	64.7	65.8	73.4	68.6	69.7	49.2
RTNet [17]	84.1	80.2	70.1	<u>79.5</u>	71.8	70.1	71.3	65.1	64.6	53.3
AMC-Net [27]	78.9	80.9	67.4	82.0	69.0	69.6	75.8	63.0	63.4	57.8
HFAN [14]	84.7	80.0	<u>72.0</u>	76.1	<u>76.0</u>	71.2	76.9	71.0	64.3	<u>61.4</u>
TMO [3]	85.7	80.0	70.1	78.0	73.6	<u>70.3</u>	76.8	66.2	58.6	47.0
DATA	<u>85.9</u>	83.6	68.4	78.4	77.2	68.3	78.0	<u>70.0</u>	59.4	64.3

4.1. Datasets

In this study, we use three datasets for network training (DUTS [23], DAVIS 2016 [15], and YouTube-VOS [26]) and three datasets for network testing (DAVIS 2016, FBMS [13], and YouTube-Objects [16]). The most popular dataset is DAVIS 2016, which consists of 30 training videos and 30 validation videos. The performance of an unsupervised VOS network is mainly evaluated on the DAVIS 2016 validation set. FBMS and YouTube-Objects are less important than DAVIS 2016, but are also widely used datasets for validating the performance of VOS models.

4.2. Evaluation Metrics

We employ three evaluation metrics in this study: region similarity \mathcal{J} , boundary accuracy \mathcal{F} , and their average \mathcal{G} . \mathcal{J} and \mathcal{F} can be calculated as follows:

$$\mathcal{J} = \frac{|M_{gt} \cap M_{pred}|}{|M_{gt} \cup M_{pred}|}, \quad (13)$$

$$\mathcal{F} = \frac{2 \times \text{Precision} \times \text{Recall}}{\text{Precision} + \text{Recall}}. \quad (14)$$

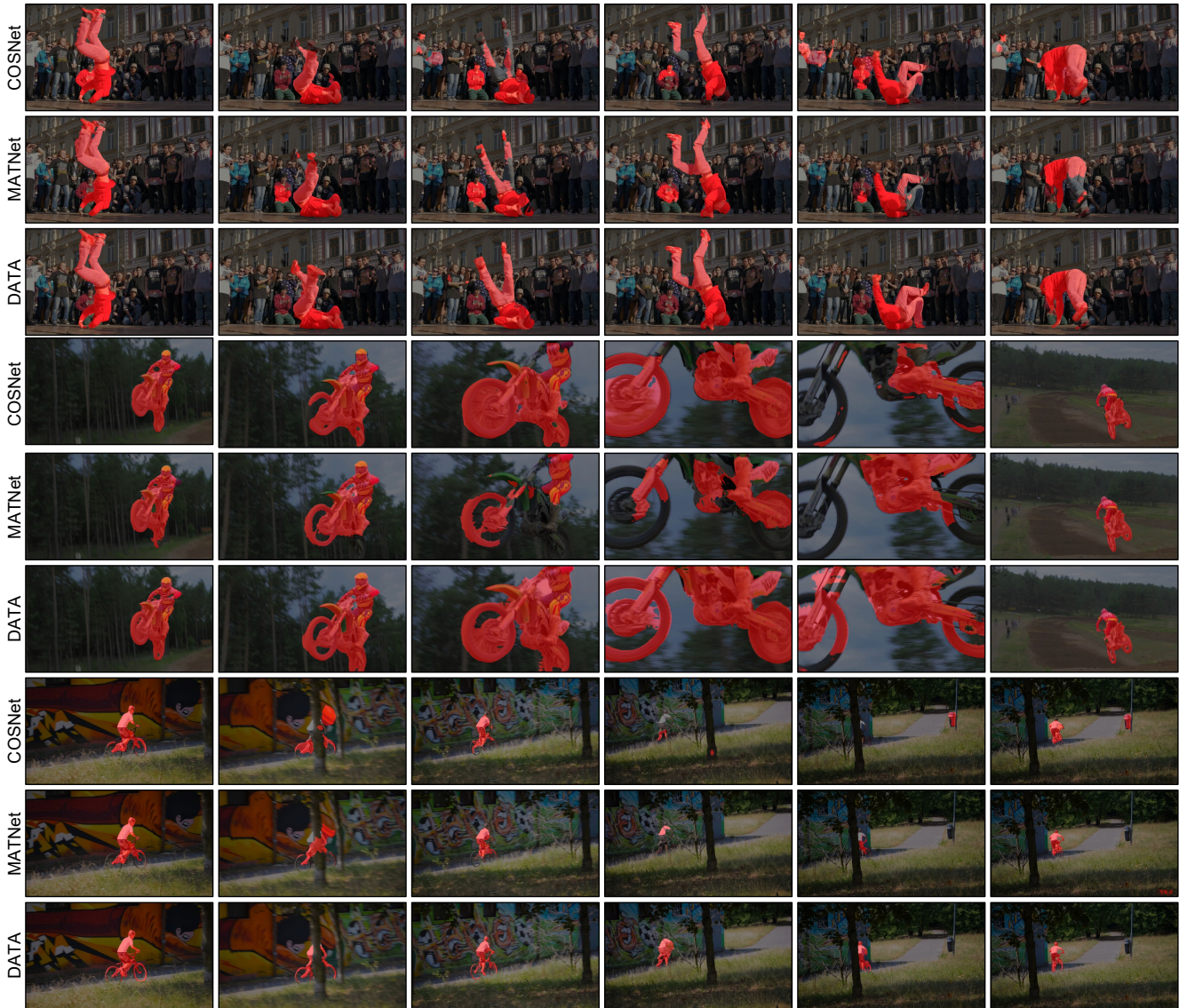


Figure 5. Qualitative comparison between DATA and other state-of-the-art methods.

For DAVIS 2016 [15] validation set, \mathcal{G} , \mathcal{J} , and \mathcal{F} are used for network evaluation, while only \mathcal{J} is used for evaluating the segmentation performance on the FBMS [13] test set and YouTube-Objects [16] dataset.

4.3. Quantitative Results

In Table 1 and Table 2, we present quantitative comparison between our proposed method and existing state-of-the-art methods on DAVIS 2016 [15] validation set, FBMS [13] test set, and YouTube-Objects [16] dataset. Our model is tested on a single GeForce RTX 3090 GPU.

DAVIS 2016. On the DAVIS 2016 validation set, the methods using predicted optical flow maps show notable performance. Specifically, PMN [7] and TMO [3] achieve

\mathcal{G}_M scores of 85.9% and 86.1%, respectively. The best performance among the existing methods is obtained by HFAN [14], which shows 87.0% on \mathcal{G}_M , 86.6% on \mathcal{J}_M , and 87.3% on \mathcal{F}_M . However, it should be considered that HFAN uses higher input resolution compared to other methods. Our proposed DATA outperforms all other methods on the same condition, i.e., input resolution. With 352×352 resolution, it achieves a \mathcal{G}_M score of 86.9%, whereas if a higher resolution of 512×512 is adopted, a \mathcal{G}_M score of 87.6% is obtained. It is also notable that while showing such satisfactory performance, the inference speed of the system is as efficient as other fast methods.

FBMS. Unlike the DAVIS 2016 validation set, the FBMS test set contains multi-object scenarios as well as single-

object scenarios. Even under this condition, DATA outperforms all other existing approaches by a reasonable margin with a \mathcal{J}_M score of 1.1%. This demonstrates that DATA is robust for videos containing multiple objects as well.

YouTube-Objects. Compared to the DAVIS 2016 validation set and FBMS test set, YouTube-Objects dataset is a much more challenging dataset. DATA surpasses other methods in these challenging cases as well. Among ten classes, DATA achieves the first place on four classes (bird, cat, dog, and train) and the second place on two classes (aeroplane and horse).

4.4. Qualitative Results

We compared DATA to COSNet [11] and MATNet [33] on DAVIS 2016 [15] validation set in Figure 5. In the first sequence, DATA keeps tracking the dancer stably, while other methods are distracted by background distractions. In the second and the third sequence, the target objects are rapidly moving and severely occluded by obstacles. Even under such conditions, DATA detects different primary objects compared to other susceptible trackers.

4.5. Analysis

In order to verify the effectiveness of the proposed components, we perform an ablation study on them, the results of which are present in Table 3. Note that the model versions for ablation study are trained and tested with 352×352 -resolution videos.

Use of DAM and TAM. To compare the model performance with and without DAM and TAM, we compare model version I, II, III, and IV. As presented in the table, DAM and TAM both bring significant performance improvements to the baseline model. When DAM is employed alone, 2.5% improvements on \mathcal{G}_M are obtained, which implies that identifying inter-relationships between RGB images and optical flow maps via domain alignment is effective for blending two distinct streams. TAM also brings meaningful improvements, \mathcal{G}_M score of 2.0%, backing up the need for global observation for specifying the primary objects. If DAM and TAM are used together, outstanding performance is obtained, \mathcal{G}_M of 86.9%. This indicates that DAM and TAM can constructively compensate each other as they focus on separate problems lying in two-stream unsupervised VOS. The qualitative effects of adopting DAM and TAM can also be found at Figure 1. In the figure, feature maps of various embedding stages are visualized. We compare four feature maps, i.e., feature maps before DAM or TAM, feature maps after DAM, feature maps after TAM, and feature maps after DAM and TAM. It can be seen that DAM and TAM are each effective for capturing and specifying the salient objects (clearer edges and higher confidence for object regions). The joint use of DAM and TAM is even

Table 3. Ablation study on the proposed components. N indicates the number of reference frames used in TAM. The models are tested on the DAVIS 2016 validation set.

Version	DAM	TAM	N	\mathcal{G}_M	\mathcal{J}_M	\mathcal{F}_M
I			-	83.4	83.2	83.5
II	✓		-	85.9	85.4	86.3
III		✓	4	85.4	85.0	85.8
IV	✓	✓	4	86.9	86.3	87.4
V	✓	✓	1	86.3	85.8	86.9
VI	✓	✓	2	86.5	86.0	87.1
VII	✓	✓	3	86.8	86.2	87.5
VIII	✓	✓	5	86.9	86.3	87.5

better than using DAM or TAM alone, validating the compatibility of the proposed modules.

Number of reference frames. As described before, TAM can take an arbitrary number of frames as reference frames given that it is based on an attention mechanism. To determine the optimal number of frames, we compare model versions that use various numbers of reference frames. As shown in model version V, VI, VII, and VIII, employing more reference frames generally leads to a higher segmentation performance. This proves that as the amount of information from a video increases, the model becomes more generalized and robust against occlusions caused by external stuffs. However, if the number of reference frames is larger than three, the performance gain is not satisfactory considering additional computations. In other words, providing semantic cues in three representative frames of a video is enough for specifying the objects for our model.

5. Conclusion

In unsupervised VOS, two-stream approaches that leverage the appearance stream and motion stream are widely used. However, existing methods do not consider the domain gap between appearance and motion features or do not efficiently leverage the temporal property of a video. Therefore, we propose two novel modules to relieve such limitations: DAM and TAM. By leveraging DAM and TAM in a collaborative manner, we achieve outstanding performance on all public benchmark datasets. Our proposed components are carefully designed, reasonable, and also effective. We believe that they will be widely adopted in many applications that require segmenting salient objects in videos.

References

- [1] D. J. Butler, J. Wulff, G. B. Stanley, and M. J. Black. A naturalistic open source movie for optical flow evaluation. In A. Fitzgibbon et al. (Eds.), editor, *European Conf. on Computer Vision (ECCV)*, Part IV, LNCS 7577, pages 611–625. Springer-Verlag, Oct. 2012.

- [2] Liang-Chieh Chen, George Papandreou, Iasonas Kokkinos, Kevin Murphy, and Alan L Yuille. Deeplab: Semantic image segmentation with deep convolutional nets, atrous convolution, and fully connected crfs. *IEEE transactions on pattern analysis and machine intelligence*, 40(4):834–848, 2017.
- [3] Suhwan Cho, Minhyeok Lee, Seunghoon Lee, Chaewon Park, Donghyeong Kim, and Sangyoun Lee. Treating motion as option to reduce motion dependency in unsupervised video object segmentation. *arXiv preprint arXiv:2209.03138*, 2022.
- [4] Ge-Peng Ji, Keren Fu, Zhe Wu, Deng-Ping Fan, Jianbing Shen, and Ling Shao. Full-duplex strategy for video object segmentation. In *Proceedings of the IEEE/CVF international conference on computer vision*, pages 4922–4933, 2021.
- [5] Diederik P Kingma and Jimmy Ba. Adam: A method for stochastic optimization. *arXiv preprint arXiv:1412.6980*, 2014.
- [6] Alex Krizhevsky, Ilya Sutskever, and Geoffrey E Hinton. Imagenet classification with deep convolutional neural networks. *Communications of the ACM*, 60(6):84–90, 2017.
- [7] Minhyeok Lee, Suhwan Cho, Seunghoon Lee, Chaewon Park, and Sangyoun Lee. Unsupervised video object segmentation via prototype memory network. *arXiv preprint arXiv:2209.03712*, 2022.
- [8] Youngjo Lee, Hongje Seong, and Euntai Kim. Iteratively selecting an easy reference frame makes unsupervised video object segmentation easier. In *Proceedings of the AAAI Conference on Artificial Intelligence*, volume 36, pages 1245–1253, 2022.
- [9] Daizong Liu, Dongdong Yu, Changhu Wang, and Pan Zhou. F2net: Learning to focus on the foreground for unsupervised video object segmentation. In *Proceedings of the AAAI Conference on Artificial Intelligence*, volume 35, pages 2109–2117, 2021.
- [10] Ilya Loshchilov and Frank Hutter. Sgdr: Stochastic gradient descent with warm restarts. *arXiv preprint arXiv:1608.03983*, 2016.
- [11] Xiankai Lu, Wenguan Wang, Chao Ma, Jianbing Shen, Ling Shao, and Fatih Porikli. See more, know more: Unsupervised video object segmentation with co-attention siamese networks. In *Proceedings of the IEEE/CVF conference on computer vision and pattern recognition*, pages 3623–3632, 2019.
- [12] Sabarinath Mahadevan, Ali Athar, Aljoša Ošep, Sebastian Hennen, Laura Leal-Taixé, and Bastian Leibe. Making a case for 3d convolutions for object segmentation in videos. *arXiv preprint arXiv:2008.11516*, 2020.
- [13] Peter Ochs, Jitendra Malik, and Thomas Brox. Segmentation of moving objects by long term video analysis. *IEEE transactions on pattern analysis and machine intelligence*, 36(6):1187–1200, 2013.
- [14] Gensheng Pei, Fumin Shen, Yazhou Yao, Guo-Sen Xie, Zhenmin Tang, and Jinhui Tang. Hierarchical feature alignment network for unsupervised video object segmentation. In *European Conference on Computer Vision*, pages 596–613. Springer, 2022.
- [15] Federico Perazzi, Jordi Pont-Tuset, Brian McWilliams, Luc Van Gool, Markus Gross, and Alexander Sorkine-Hornung. A benchmark dataset and evaluation methodology for video object segmentation. In *Proceedings of the IEEE Conference on Computer Vision and Pattern Recognition*, pages 724–732, 2016.
- [16] Alessandro Prest, Christian Leistner, Javier Civera, Cordelia Schmid, and Vittorio Ferrari. Learning object class detectors from weakly annotated video. In *2012 IEEE Conference on computer vision and pattern recognition*, pages 3282–3289. IEEE, 2012.
- [17] Sucheng Ren, Wenxi Liu, Yongtuo Liu, Haoxin Chen, Guoqiang Han, and Shengfeng He. Reciprocal transformations for unsupervised video object segmentation. In *Proceedings of the IEEE/CVF conference on computer vision and pattern recognition*, pages 15455–15464, 2021.
- [18] Christian Schmidt, Ali Athar, Sabarinath Mahadevan, and Bastian Leibe. D2conv3d: Dynamic dilated convolutions for object segmentation in videos. In *Proceedings of the IEEE/CVF Winter Conference on Applications of Computer Vision*, pages 1200–1209, 2022.
- [19] Mennatullah Siam, Chen Jiang, Steven Lu, Laura Petrich, Mahmoud Gamal, Mohamed Elhoseiny, and Martin Jagersand. Video object segmentation using teacher-student adaptation in a human robot interaction (hri) setting. In *2019 International Conference on Robotics and Automation (ICRA)*, pages 50–56. IEEE, 2019.
- [20] Karen Simonyan and Andrew Zisserman. Very deep convolutional networks for large-scale image recognition. *arXiv preprint arXiv:1409.1556*, 2014.
- [21] Hongmei Song, Wenguan Wang, Sanyuan Zhao, Jianbing Shen, and Kin-Man Lam. Pyramid dilated deeper convlstm for video salient object detection. In *Proceedings of the European conference on computer vision (ECCV)*, pages 715–731, 2018.
- [22] Zachary Teed and Jia Deng. Raft: Recurrent all-pairs field transforms for optical flow. In *European conference on computer vision*, pages 402–419. Springer, 2020.
- [23] Lijun Wang, Huchuan Lu, Yifan Wang, Mengyang Feng, Dong Wang, Baocai Yin, and Xiang Ruan. Learning to detect salient objects with image-level supervision. In *CVPR*, 2017.
- [24] Wenguan Wang, Xiankai Lu, Jianbing Shen, David J Crandall, and Ling Shao. Zero-shot video object segmentation via attentive graph neural networks. In *Proceedings of the IEEE/CVF international conference on computer vision*, pages 9236–9245, 2019.
- [25] Wenguan Wang, Hongmei Song, Shuyang Zhao, Jianbing Shen, Sanyuan Zhao, Steven CH Hoi, and Haibin Ling. Learning unsupervised video object segmentation through visual attention. In *Proceedings of the IEEE/CVF Conference on Computer Vision and Pattern Recognition*, pages 3064–3074, 2019.
- [26] Ning Xu, Linjie Yang, Yuchen Fan, Dingcheng Yue, Yuchen Liang, Jianchao Yang, and Thomas Huang. Youtube-vos: A large-scale video object segmentation benchmark. *arXiv preprint arXiv:1809.03327*, 2018.
- [27] Shu Yang, Lu Zhang, Jinqing Qi, Huchuan Lu, Shuo Wang, and Xiaoxing Zhang. Learning motion-appearance

- co-attention for zero-shot video object segmentation. In *Proceedings of the IEEE/CVF International Conference on Computer Vision*, pages 1564–1573, 2021.
- [28] Zhao Yang, Qiang Wang, Luca Bertinetto, Weiming Hu, Song Bai, and Philip HS Torr. Anchor diffusion for unsupervised video object segmentation. In *Proceedings of the IEEE/CVF International Conference on Computer Vision*, pages 931–940, 2019.
- [29] Yuhui Yuan, Xilin Chen, and Jingdong Wang. Object-contextual representations for semantic segmentation. In *European conference on computer vision*, pages 173–190. Springer, 2020.
- [30] Kaihua Zhang, Zicheng Zhao, Dong Liu, Qingshan Liu, and Bo Liu. Deep transport network for unsupervised video object segmentation. In *Proceedings of the IEEE/CVF International Conference on Computer Vision*, pages 8781–8790, 2021.
- [31] Lu Zhang, Jianming Zhang, Zhe Lin, Radomír Měch, Huchuan Lu, and You He. Unsupervised video object segmentation with joint hotspot tracking. In *European Conference on Computer Vision*, pages 490–506. Springer, 2020.
- [32] Mingmin Zhen, Shiwei Li, Lei Zhou, Jiayang Shang, Haoan Feng, Tian Fang, and Long Quan. Learning discriminative feature with crf for unsupervised video object segmentation. In *European Conference on Computer Vision*, pages 445–462. Springer, 2020.
- [33] Tianfei Zhou, Shunzhou Wang, Yi Zhou, Yazhou Yao, Jianwu Li, and Ling Shao. Motion-attentive transition for zero-shot video object segmentation. In *Proceedings of the AAAI Conference on Artificial Intelligence*, volume 34, pages 13066–13073, 2020.